OPTIMIZATION DESIGN OF TANGENTIAL FLOW-TRANSVERSE AXIAL FLOW DOUBLE DRUM MAIZE THRESHING DEVICE BASED ON EDEM
/
基于 EDEM 的切流-横轴流双滚筒玉米脱粒装置的优化

Le LI[1,2)], Yang ZHOU[1,2)], Junshan NIE[1)], Qiqiang LI[1)], Lihua ZHANG[1,*)]
[1)]College of Mechanical and Electrical Engineering, Sichuan Agricultural University, Yaan / China;
[2)]Le LI and Yang ZHOU should be considered joint first author
E-mail: zhanglihua69@126.com
DOI: https://doi.org/10.35633/inmateh-77-53

Keywords: *high moisture content maize threshing, flexible concave sieve, inter-drum clearance, MBD-EDEM co-simulation, structural design*

ABSTRACT
To address the problems of high kernel breakage rate and high unthreshed rate during direct maize kernel harvesting under conditions of high moisture content and dense planting - common in the single longitudinal axial-flow harvesters widely used in Southwest China - a tangential–transverse axial-flow double-drum maize threshing device was designed and optimized. The drum combination configuration was determined through theoretical analysis, and the influence of the vertical spacing between the two drums on threshing performance was investigated. The flexible concave screen and transition sieve plate were also redesigned. Using EDEM and Adams software, the threshing process was simulated and analysed to verify the rationality of the design. A prototype was fabricated, and drum speed, deflection angle, and feeding rate were selected as test factors. A response surface experiment was conducted with kernel breakage rate and unthreshed rate as evaluation indices. Multi-objective optimization of the regression model was performed using the response surface methodology (RSM). After rounding, the optimal parameter combination was determined as follows: drum speed of 453 r/min, deflection angle of 69°, and feeding rate of 6.7 kg/s. Verification tests yielded a kernel breakage rate of 2.76% and an unthreshed rate of 0.11%, meeting production requirements and providing a valuable reference for the design of maize threshing devices in Southwest China.

摘要
针对西南地区普遍应用的单纵轴流机型在高含水率密植条件下玉米籽粒直收存在的破碎较高、未脱净率较高问题，设计切流-横轴流双滚筒玉米脱粒装置并进行优化设计，通过理论分析确定滚筒的组合方式，研究两滚筒间垂直高度对脱粒的影响，并对柔性凹板筛、过渡筛板进行重新设计，采用 EDEM、Adams 对脱粒过程进行仿真分析验证设计的合理性。搭建样机，选取滚筒转速、导流角、喂入量为试验因素，以破碎率和未脱净率为试验指标开展响应面试验，基于响应曲面法对回归模型进行多目标优化，得到最优参数圆整后的组合为：滚筒转速 453r/min、导流角为 69°、喂入量为 6.7kg/s，验证试验测得玉米破碎率 2.76%，未脱净率为 0.11%，满足生产需求，可为西南地区的脱粒装置设计提供参考。

INTRODUCTION
Limited by geographical conditions, small and medium-sized machines are widely used for maize harvesting in southwest China at this stage. Such machines are mostly longitudinal axial flow drums. Due to the limitation of models, such drums are generally small in size. When harvesting maize under high water content and dense planting conditions, due to the short movement stroke of maize inside the drum, the non-removal rate is high. In order to ensure the removal rate, it is often achieved by increasing the working speed *(Cui et al., 2019)*. Although the feeding rate is increased to a certain extent, it also brings a higher breakage rate *(Wang et al., 2023; Wang et al., 2021; Li et al., 2023)*, which is not suitable for the development requirements of modern and efficient harvesting.

Scholars both in China and abroad have conducted relevant research on threshing devices to address the problems of high grain breakage rates and high unthreshed grain rates. *Steponavičius et al., (2018, 2017*), used a high-speed camera to conduct a control test of high-moisture maize threshing on different concave plates of a tangential flow maize thresher.

It was found that the average speed of maize ears in the threshing gap and the number of shocks to maize ears increased with the increase of the linear speed of the threshing element. *Poustovit & Katkov, (2016),* selected maize with moisture content of 32.5 % and 18.5 % to carry out control experiments with different feeding methods, and demonstrated that the advantages of maize ear feeding parallel to the threshing cylinder axis are greater than vertical feeding, and the high-humidity maize is more than 30 % higher than the unthreshed rate of ordinary maize. *Li et al., (2014, 2015) and Li & Lei, (2017)*, found that the structural pattern is a key factor influencing the discrete behaviour of maize kernels, and that the kernels in the middle of the ear strictly follow this pattern. *Wang et al., (2021), Zhou et al., (2005) and Li et al., (2023),* found that the optimal maize threshing method is based on the principles of extrusion and rubbing, with ears fed in an orderly manner to ensure that maize kernels are subjected to lateral stress as much as possible. *Yang et al., (2018),* improved a double-drum threshing device based on the Xinjiang-2 machine model, featuring a nail-tooth drum combined with a mixed nail-tooth and plate-tooth drum. The study found that this structure exhibits good adaptability to maize with high moisture content and large feeding rates. In summary, to improve the quality of maize threshing, it is necessary to consider factors such as the combination of threshing drums, feeding direction, low-loss threshing components, and concave screen configuration.

In this paper, a tangential-transverse axial flow drum maize threshing device was designed to address the challenges of direct kernel harvesting of high-moisture maize under dense planting conditions in Southwest China. The key factors influencing the threshing performance were analysed to provide new insights for improving direct grain harvesting in the region.

MATERIAL AND METHODS

Overall structure and working principle

The tangential-transverse axial flow drum threshing device is based on the 4LZ-5.0S model. It mainly consists of two parts: a front tangential flow drum and a rear transverse axial flow drum. The overall structure is shown in Figure 1. The tangential flow drum has a diameter of 520 mm and a length of 650 mm, while the transverse axial flow drum has a diameter of 520 mm and a length of 1290 mm.

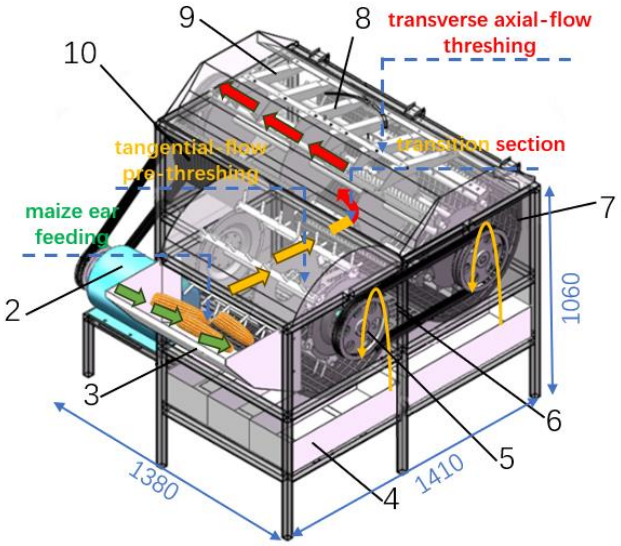

Fig. 1 - Structure of the tangential-transverse axial flow maize threshing device

1. Tangential flow drum; 2. Motor; 3. Feeding inlet; 4. Feeding box; 5. Pulley; 6. Transition sieve plate; 7. Flexible concave sieve; 8. deflection angle adjustment mechanism; 9. Transverse axial flow drum; 10. Cylindrical concave sieve

During the operation, the material enters from the feeding inlet. Under the action of the tangential threshing device, part of the kernels are threshed and separated by the tangential concave plate sieve. The tangential threshing device bears the function of feeding and pre-threshing. At the same time, the material is grabbed by the tangential flow drum to form a more uniform material layer, and is thrown to the side of the transverse axial flow threshing device under the action of the threshing element. In the transverse axial flow threshing device, the material moves backward along the axial direction of the drum with the rotation of the drum, and completes the subsequent threshing and separation under the strike and rubbing of the threshing element.

Loss reduction mechanism and key component design

Loss reduction mechanism

The kernels on the cob are tightly arranged, forming a compact and cohesive ear. This structural pattern among the kernels gives the ear a strong binding effect, making complete ears significantly more difficult to thresh than those in which this structure has already been disrupted. However, the structural pattern among kernels is not uniform, resulting in uneven threshing forces across different parts of the ear (*Xing et al., 2024*). Therefore, by first disrupting the assembly structure among the kernels and subsequently threshing using less aggressive ridge elements, threshing efficiency and operational quality can be greatly improved. The threshing process is illustrated in Fig 2.

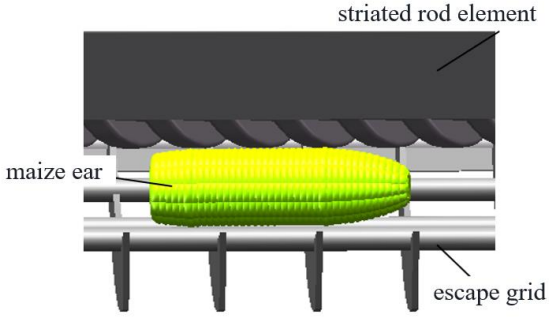

Fig. 2 - Contact diagram between the maize ear-rasp bar threshing element and the concave plate screen

For the convenience of analysis, the ear is regarded as a regular cylinder. When the threshing element collides with the ear, the pressure can be expressed as:

$$m_1 \frac{dv_i}{dt} = m_2 \frac{dv_j}{dt} = P_{ij} \tag{1}$$

The threshing element collides with the maize ear, causing local compression at the point of contact and resulting in a relative compression displacement denoted by ε. The critical velocity of the two interacting bodies can be derived as follows:

$$\dot{\varepsilon} = v_i + v_j \tag{2}$$

The contact area between the threshing element and the maize ear can be approximated as an elliptical surface, which can be expressed as:

$$s = qr \tag{3}$$

where:

$$\begin{cases} q = \left[\frac{3\pi}{2} P_{ij} (k_1 + k_2) \eta_R \right]^{1/3} \\ r = \left[\frac{3\pi}{2} P_{ij} (k_1 + k_2) \eta_R \right]^{1/3} \end{cases} \tag{4}$$

In the formula, η_R represents the factor influencing the radius of curvature, k_1 and k_2 denote the characteristic parameters of the threshing element and the elastic properties of the maize ear, respectively.

The calculation formula is:

$$\begin{cases} \frac{1}{\eta_R} = \frac{1}{R_1'} + \frac{1}{R_1''} + \frac{1}{R_2'} + \frac{1}{R_2''} \\ k_1 = \frac{1-\mu_1}{\pi E_1} \\ k_2 = \frac{1-\mu_2}{\pi E_2} \end{cases} \tag{5}$$

R_1' is the maximum curvature radius of the threshing element in any normal plane of the contact area, R_1'' is the minimum curvature radius of the threshing element in any normal plane of the contact area, R_2' is the maximum curvature radius of the threshing element in any normal plane of the contact area, R_2'' is the minimum curvature radius of the threshing element in any normal plane of the contact area. Based on Hertz contact theory, the contact pressure P_0 between threshing element and the maize ear can be expressed as:

$$P_0 = n\varepsilon^{3/2} \tag{6}$$

$$n = \left[\frac{16}{3\pi(k_1+k_2)}\right]\sqrt{\frac{\eta_R}{s^3}} \tag{7}$$

Differentiating equation (2) and combining the result with equation (1), then substituting into (6) yields:

$$\dot{\varepsilon} = n(\frac{1}{m_1}+\frac{1}{m_2})\varepsilon^{3/2} \tag{8}$$

By multiplying $\dot{\varepsilon}$ on both sides of the above equation and integrating, the following expression is obtained:

$$(\dot{\varepsilon}^2 - v^2) = -\frac{4}{5}\frac{(m_1+m_2)n\varepsilon^{5/2}}{m_1m_2} \tag{9}$$

where v is the initial collision velocity between the threshing element and the maize ear. During the threshing process, the maximum deformation of the ear occurs when its acceleration equals 0. By combining equations (7) and (9), the maximum contact pressure between the threshing element and the maize ear at any contact point can be obtained.

$$P_{\max} = \left\{\left[\frac{16}{3\pi(k_1+k_2)}\right]\sqrt{\frac{\eta_R}{s^3}}\right\}^{2/5}(\frac{5m_1m_2v^2}{4(m_1+m_2)})^{3/5} \tag{10}$$

Combining with the surface pressure equation yields:

$$P_1 = \frac{1}{\pi^{4/3}}\left\{\left[\frac{\left(\frac{3}{2\pi}\right)^{1/3}n^{2/15}}{mr\left[\left(k_1+k_2\right)\eta_R\right]^{2/3}}\right]\left(\frac{5m_1m_2v^2}{4(m_1+m_2)}\right)^{1/5}\right\} \tag{11}$$

It can be seen that the maximum contact pressure experienced by the maize ear is directly related to its deformation, which is influenced by factors such as the mass of the threshing element, the mass of the ear, the contact area, and the collision velocity. Therefore, when the mass of the threshing element and the ear remain constant, reducing the collision velocity and increasing the contact area can effectively reduce kernel breakage. Considering the mechanical interactions between kernels, the conditions for kernel detachment under the support of multiple kernels can be expressed as follows:

$$P_1 > nF_d \tag{12}$$

where n is the number of kernels in contact with the threshing element, and n reaches its maximum value when the ear remains intact. F_d is the threshing force required for a single kernel. It can be inferred that threshing becomes easier once the assembly pattern of kernels is disrupted, allowing for lower-loss threshing when using a combination of segmentation and threshing elements.

Key component design

Design of Double Drum Position Parameters

The vertical distance between the tangential flow drum and the transverse axial flow drum is one of the key parameters affecting the entire threshing process (*Wang et al., 2021*). Therefore, it is particularly important to determine the positional parameters between the two drums and to optimize the structural design of the transition sieve plate. The movement of the maize ear during the transition process is illustrated in Fig. 3. After being impacted by the tangential flow drum, the ear moves at high speed and strikes the transition plate, where its velocity decreases, and its direction changes. A force analysis is then conducted for this impact condition.

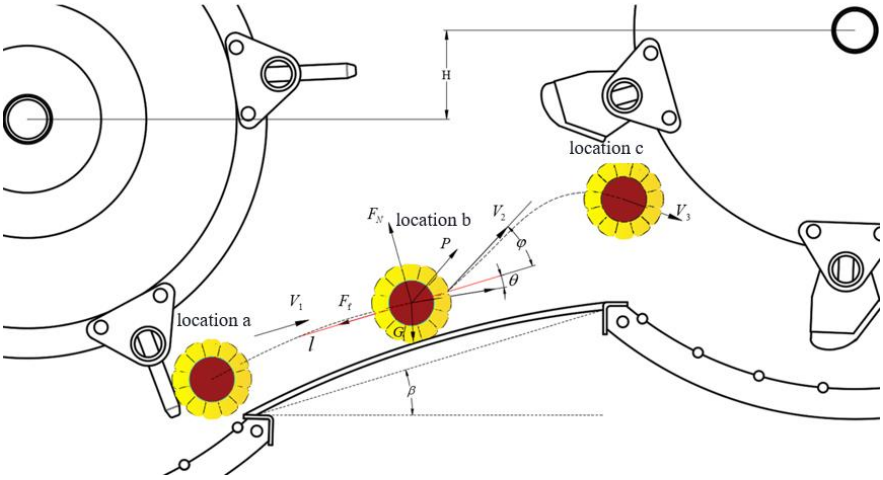

Fig. 3 - Diagram of ear movement and force analysis at the transition

The angle between the collision line l and the horizontal plane is expressed as:

$$\beta = \arcsin\frac{H}{l} \tag{13}$$

The positive direction is defined as rightward along the impact line l and vertically upward perpendicular to the impact line. The momentum balance equation of the ear from position a to b can be obtained through momentum decomposition:

$$\begin{cases} m_2 v_1 \cos\theta - m_2 v_{2x} = \int_0^{\Delta t} F_x dt \\ -m_2 v_1 \sin\theta + m_2 v_{2y} = \int_0^{\Delta t} F_y dt \end{cases} \tag{14}$$

where F_x and F_y are the components of the total force acting on the ear at position b, respectively. Based on the force analysis, the following relationship can be obtained:

$$\begin{cases} F_x = P\cos\varphi - G_1\sin\theta - F_f \\ F_y = P\sin\varphi + F_N - G_1\cos\theta \end{cases} \tag{15}$$

By combining these equations, we obtain:

$$v_2 = \sqrt{\left[\frac{m_2 v_1\cos\theta - \Delta t(m_2\cos\varphi - m_2 g - F_f)}{m_2}\right]^2 + \left[\frac{m_2 v_1\sin\theta + \Delta t(P\sin\varphi + F_N - m_2 g)}{m_2}\right]^2} \tag{16}$$

According to the law of conservation of kinetic energy, the kinetic energy balance equation for the ear at position c at a certain moment after being ejected, can be expressed as:

$$\frac{1}{2}m_2 v_2^2 = m_2 gh + \frac{1}{2}m_2 v_3^2 \tag{17}$$

Thus, the velocity of the ear at position c is obtained. In the formula, m_2 is the ear weight; v_1 is the ejection velocity of the ear from the tangential flow drum; v_2 is the rebound velocity of the ear after impacting the transition plate; v_3 velocity of the ear at a given moment after rebound; θ is the angle between the v_1 direction and the collision line; φ is the angle between the v_2 direction and the collision line; P is the collision reaction force; F_N is the support force; Δt is the collision duration.

In summary, when the material properties remain constant, the movement of the ear between the two drums is primarily influenced by the angle between the transition sieve plate and the collision line, which corresponds to the vertical distance between the two drums. Variations in this vertical distance have a significant effect on the ear's post-collision motion - including its direction, velocity, and rebound height. Additionally, collisions among ears can result in excessive momentum loss, thereby reducing the smoothness of material flow between the two drums during the maize threshing process.

To achieve the optimal threshing performance, and considering that an excessively large vertical distance may hinder smooth material transport, the vertical distance *H* was set within the range of 0~75 mm, while the horizontal spacing of the sieve plate between the two drums was maintained at 270 mm.

Design of the transition sieve plate

The transition sieve plate serves a dual purpose: it screens out detached maize kernels while working in coordination with the drum to ensure smooth material flow during threshing. In this study, two types of transition sieve plates were designed - a curved transition sieve plate and a straight transition sieve plate - as shown in Figures 4 and 5. To allow the maize ears to fall naturally with minimal kinetic disturbance, the inclination angle of the sieve plate was set greater than the minimum rolling friction angle of the maize ear on 45steel. In this design, the curvature angle of the arc plate is 18°, and the sieve openings are 15 × 15 mm square holes. The optimal structural configuration and installation position were determined through simulation analysis.

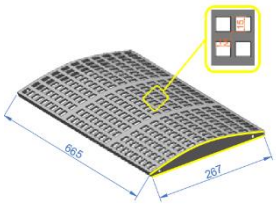

Fig. 4 - Curved transition sieve plate

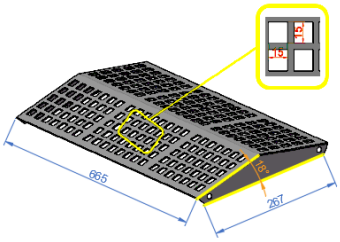

Fig. 5 - Straight transition sieve plate

Design of flexible concave sieve

The structure of the flexible concave sieve is illustrated in Figures 6 and 7. It consists of two pairs of buffer springs, spring seats, a circular-tube concave sieve, and hinged connecting rods. This configuration enables the sieve to absorb impact forces exerted by the maize ears and to adaptively adjust the threshing gap when the feeding volume is high or the material is unevenly distributed.

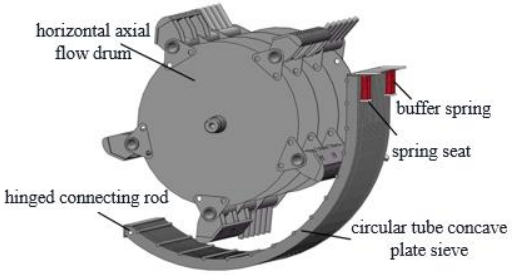

Fig. 6 - Structural diagram of the flexible concave sieve

Fig. 7 - Physical model of the flexible concave sieve

Based on previous studies and physical test data, the threshing force range for high-moisture maize is 2~40.6 N, while the kernel crushing force range is 109.8~247.4 N. In this study, the average values were adopted for calculation. The impact force between the maize ear and the circular-tube concave sieve during threshing was approximately 252 N. Therefore, the maize ear experiences a collision force greater than the maximum threshing force but lower than the minimum crushing force, ensuring effective threshing without kernel damage.

The simplified force analysis of the ear during the threshing process is shown in Fig. 8, and the required spring force can be calculated using the following equation:

$$F_k = F_g \cos\theta + G_1 + G_2 = (F_p - F_{w\min}) \cos\theta + G_1 + G_2 \quad (18)$$

In the formula, F_k is the spring force required according to the loss reduction theory; F_g is the contact collision force acting on the ear; G_1 is weight of the ear; G_2 is the weight of the concave sieve; α is the angle between the impact force direction and the vertical. When the directions of the contact collision force F and the spring force are aligned on the same axis, that is $\alpha = 0$, the spring force reaches its maximum value.

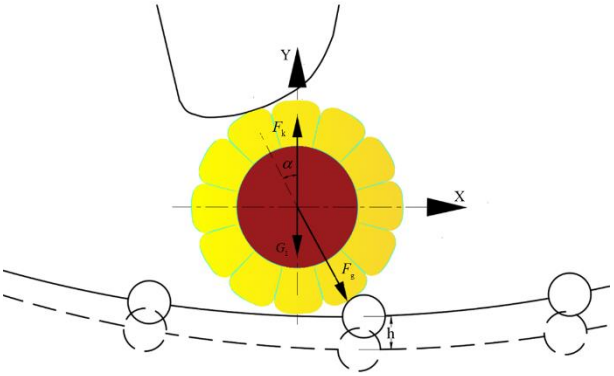

Fig. 8 - Contact diagram of the flexible concave sieve, ear, and threshing element

The weight of the concave plate is 14.3 kg, and the maximum spring force required is calculated to be 288.2 N. Accordingly, the maximum force of a single spring can be determined as follows:

$$F_0 = \mathrm{k}h_{\max} = \frac{F_{\mathrm{k}}}{4} = 72.05N \tag{19}$$

where F_0 is the maximum force of a single spring; k is the spring stiffness; $h_{\max}$ is the maximum compression of the spring (the maximum downward displacement of the concave sieve). To prevent adverse effects on threshing performance or potential mechanical damage caused by excessive changes in the concave sieve gap due to over-compression, spring seats are installed to limit the maximum compression. The maximum spring displacement $h_{\max}$ is set to 8 mm. Based on this, when the spring stiffness is 9 N/mm, the design requirements are satisfied.

Simulation settings

Simulation of different drum vertical heights and transition plates on material flow

Based on the measured physical parameters and mechanical properties of maize *(Han et al., 2024)*, a discrete element threshing model of the ear's midsection was established in EDEM *(Yu et al., 2015)*, as shown in Fig. 9. The effects of varying drum heights on material flow were simulated and analysed. The transition plate was designed as an arc panel, and simulations were conducted for vertical height differences of 0, 25, 50, and 75 mm between the drums. The drum rotational speed was set to 420 r/min, and a specified number of maize ears were introduced at the transition zone. A monitor, as shown in Fig. 10, was used to record the real-time number of ears at the transition during the threshing process to evaluate material flow fluency.

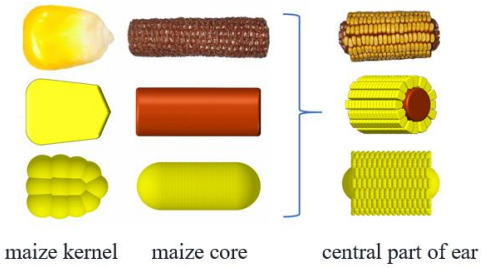

Fig. 9 - Discrete element modelling process of the middle section of a maize ear

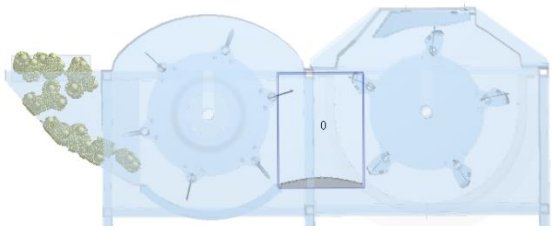

Fig. 10 - Setup of the monitoring system for counting the number of ears

Simulation of the flexible concave sieve based on DEM–MBD coupling

To evaluate the influence of the flexible concave sieve on threshing quality, a coupled EDEM-ADAMS simulation was conducted. The coupling enabled analysis of ear-threshing behaviour under the action of the buffering spring force. In ADAMS, the constraints and motions of each component were defined individually. The drum rotational speed was set to 420 r/min, and a revolute pair was applied between the flexible concave sieve and the hinged rod, allowing the sieve to pivot along the hinge when impacted by maize ears. Additionally, four spring forces were assigned to the flexible concave sieve, and GForce functions were applied to all load-bearing components of the threshing device to ensure two-way data transmission between ADAMS and EDEM. In EDEM, maize ear particles were added, and material properties were defined. The feeding speed of the ears was set to 8 kg/s, with a total feeding mass of 10 kg.

During post-processing, the simulation time step was set as an integer multiple of that in ADAMS. The coupling interface was activated, and the linking files were adjusted accordingly. The two-phase co-simulation was then executed within the Co-Simulation module of ADAMS. The resulting coupled simulation model is shown in Figs. 11 and 12.

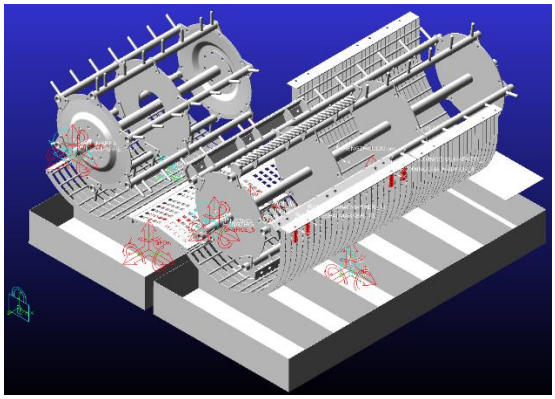

Fig. 11 - Simulation model in ADAMS

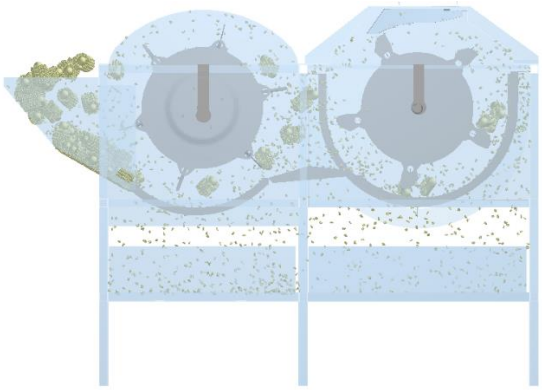

Fig. 12 - Simulation model in EDEM

Bench verification test

Referring to the "Threshing machine test method" *(GB / T 5982-2017) (SAC/TC 201, 2017)* and the "National standard for maize harvesting machinery" *(GB / T 21962-2020) (SAC/TC 201, 2020)*, Zhenghong 507, a maize variety widely cultivated in Sichuan, was selected as the test material. The grain moisture content was maintained at 30% ± 1%. A three-factor and three-level response surface experiment was designed to identify the optimal operating parameters and validate the results. The experimental threshing bench used for testing is shown in Fig. 13.

Fig. 13 - Test bench

RESULTS

Effect of drum vertical height and transition plate on material flow

The feeding rate of maize ears was set at 8 kg/s, with a total feeding mass of 10 kg. As shown in Fig. 14, a significant accumulation of ears occurred between 1–3 s at the transition section due to the large feeding volume and repeated impacts from the drum. After 3 s, under the continued action of the drum, the number of ears at different vertical drum heights showed a rapid decreasing trend. Among the tested configurations, a vertical height of 25 mm resulted in the fastest decrease in ear count and the lowest number of ears recorded by the monitoring system. Additionally, at 8 s after threshing, this configuration left the smallest amount of residual material. In contrast, when the vertical height was 75 mm, the rate of decrease was the slowest, material accumulation was greater, and the residual quantity on the mandrel after threshing was the highest. Notably, as shown in Fig. 14, the statistical count at 75 mm exhibited a marked rebound around 6 s, indicating repeated ear collisions and unstable material flow.

It is inferred that when the vertical height between the drums is excessively large, the inclination angle of the collision line also increases, causing more ears to rebound toward the tangential flow drum or become over-deflected, leading to repeated impacts by the transverse axial flow drum and resulting in material congestion. This demonstrates that the vertical height has a significant effect on threshing flow stability. Therefore, in this study, the optimal vertical height was determined to be 25 mm, corresponding to a transition plate installation angle of 5.3°.

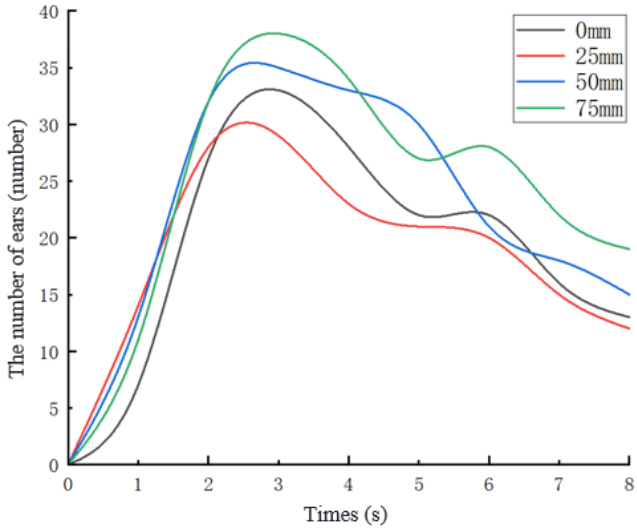

Fig. 14 - Variation in the number of maize ears at the transition section under different vertical drum heights

Considering the installation angle, to ensure that the ears on both sides of the straight transition plate fall naturally, the bending angle at the centre of the plate was set to 150°. A comparison of the material flow between the curved transition plate and the straight transition plate was conducted, as shown in Fig. 15. In the figure, the A-series represents the curved transition plate, while the B-series represents the straight transition plate. Observation of the ear motion between 2 s and 6 s indicates that, due to differences in the installation position of the transition plates and the collision angles of the ears, both the movement direction and rebound height varied noticeably. Unthreshed ears tended to remain longer on the curved transition plate, exhibiting a slower flow velocity compared to the straight transition plate. Combined with the data recorded by the monitoring system, it was found that the straight transition plate demonstrated better material flow performance than the curved transition plate.

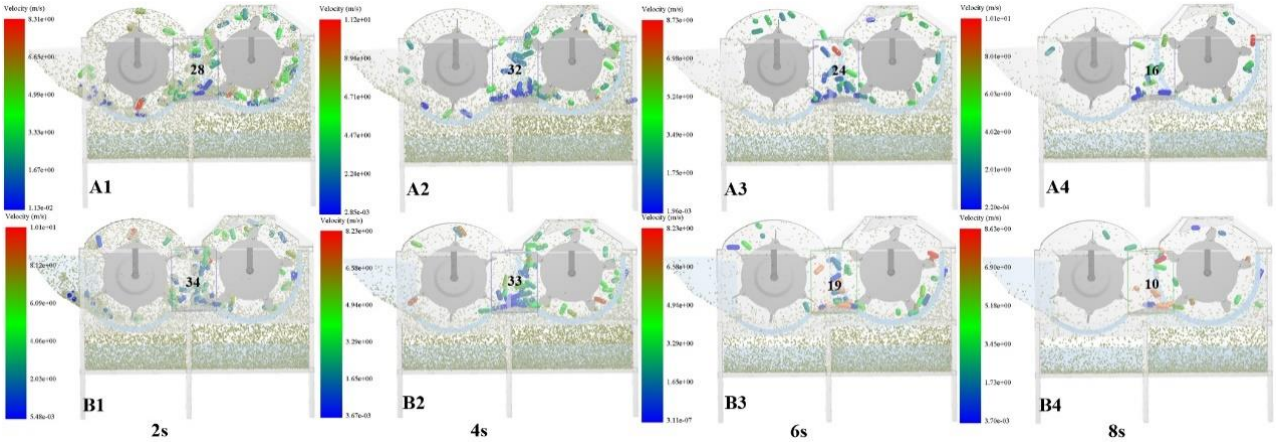

Fig. 15 - Comparison of different transition plates

Simulation analysis of the flexible concave sieve based on DEM-MBD

The simulation process of maize threshing with and without the flexible concave sieve is shown in Fig. 16 and Fig. 17. After feeding, the maize ears are initially threshed by the tangential flow drum and then transferred to the transverse axial flow drum for further threshing. Through the combined action of the concave sieve and threshing rod elements, extensive threshing occurs. When the ears impact the flexible concave sieve, the buffer springs compress slightly to absorb part of the impact energy.

Due to this buffering effect, the flow speed of the ears in the threshing chamber becomes slightly slower than in the conventional threshing process without buffering; however, this does not impede the smooth movement of the ears within the drum. The flexible concave sieve allows the ears to be more evenly rubbed by the rod elements, which helps reduce kernel breakage and improve the overall threshing rate.

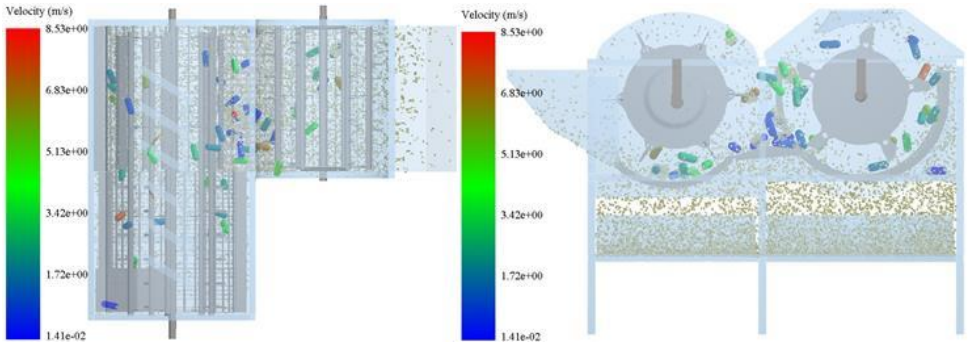

Fig. 16 - Threshing process using a flexible concave sieve

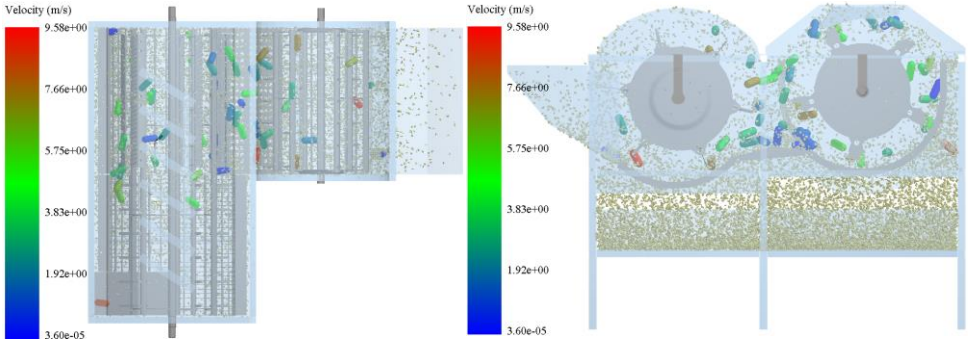

Fig. 17 - Threshing process using a conventional cylindrical concave sieve

During the maize threshing process, the displacement variation of the buffer spring is shown in Fig. 18, with a maximum displacement of 7.23 mm, remaining within the designed compression limit. Frequency band analysis of the concave sieve displacement indicates that the buffer spring displacement generally ranges between 3 mm and 5 mm, demonstrating that the flexible concave sieve effectively absorbs part of the impact force exerted by the maize in the threshing section. The relatively uniform number of maize ears entering the threshing area contributes to reducing kernel breakage and unthreshed grains caused by uneven feeding or excessive impact.

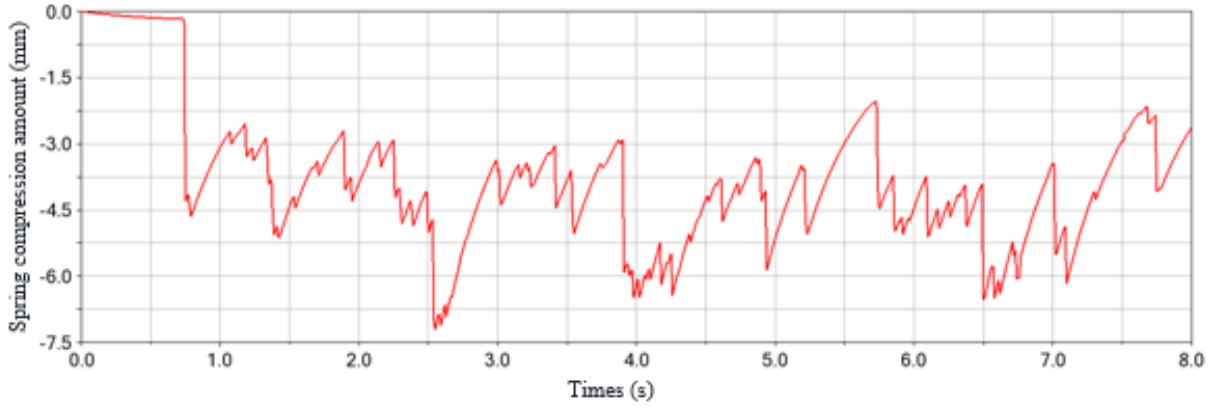

Fig. 18 - Change in spring compression during the threshing process

Compared with the kernel stress distribution with and without the buffer spring, as shown in Fig. 19, the number of stress peaks in the case of the flexible concave sieve is notably smaller. The maximum peak force is 1010.8 N, which is 27.6% lower than the maximum peak force of 1395.9 N observed with the cylindrical concave sieve. Similarly, the average kernel force is 118.6 N, representing a 10.08% reduction compared to 131.9 N for the cylindrical concave sieve. These results indicate that the flexible concave sieve provides superior buffering performance, effectively reducing the impact force exerted on the maize kernels during threshing.

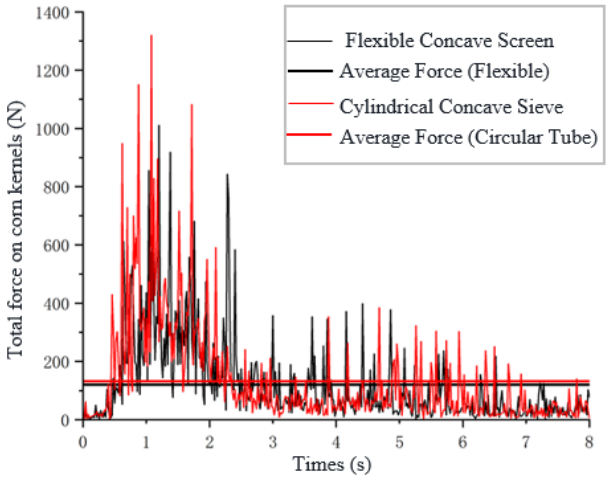

Fig. 19 - Kernel force with and without buffer spring

Response surface test

Using drum speed (A), deflection angle (B), and feeding rate (C) as independent variables, and the kernel breakage rate and unthreshed rate of maize as response variables, an experimental design was conducted using Design-Expert 13. The regression models for breakage rate (Sw) and unthreshed rate (SP) were analysed. The levels of each factor are presented in Table 1, and the experimental results are shown in Table 2. Variance analysis of the regression equations for breakage rate and unthreshed rate was performed using Design-Expert statistical software, and the results are summarized in Table 3.

Table 1

Test factor coding

Level	Drum speed [r/min]	Deflection angle [°]	Feeding rate [kg/s]
-1	420	50	6
0	470	60	7
1	520	70	8

Table 2

Response surface test design and results

No.	A drum speed	B deflection angle	C feeding rate	Breakage rate [%]	Unthreshed rate [%]
1	-1	-1	0	2.15	1.42
2	1	-1	0	3.82	0
3	-1	1	0	2.53	0.33
4	1	1	0	5.03	0
5	-1	0	-1	2.75	0.72
6	1	0	-1	4.36	0
7	-1	0	1	2.38	0.98
8	1	0	1	5.13	0
9	0	-1	-1	2.62	0.58
10	0	1	-1	3.16	0.08
11	0	-1	1	2.51	0.96
12	0	1	1	4.14	0.11
13	0	0	0	2.58	0.31
14	0	0	0	2.63	0.26
15	0	0	0	2.55	0.22

No.	A drum speed	B deflection angle	C feeding rate	Breakage rate [%]	Unthreshed rate [%]
16	0	0	0	2.76	0.21
17	0	0	0	2.32	0.19

Table 3

Analysis of variance of regression equation between breakage rate and unthreshed rate

Source of variance	breakage rate					unthreshed rate				
	Sum of square	df	F value	P value	Signifi-cance	Sum of square	df	F value	P value	Signifi-cance
Model	14.79	9	65.06	< 0.001	**significant**	2.77	9	104.13	< 0.0001	**significant**
A	9.10	1	359.99	< 0.001	**	1.49	1	504.22	< 0.001	**
B	1.77	1	69.65	< 0.001	**	0.7442	1	252.21	< 0.001	**
C	0.2016	1	7.98	0.026	*	0.0561	1	19.02	0.003	**
AB	0.1722	1	6.82	0.035	*	0.2970	1	100.66	< 0.001	**
AC	0.3249	1	12.86	0.009	**	0.0169	1	5.73	0.048	*
BC	0.2970	1	11.76	0.011	*	0.0306	1	10.38	0.015	*
A2	1.95	1	77.29	< 0.001	**	0.0388	1	13.15	0.008	**
B2	0.075	1	2.97	0.129	-	0.0451	1	15.29	0.0066	*
C2	0.694	1	27.47	0.001	**	0.0349	1	11.82	0.011	*
Residual	0.1769	7				0.0207	7			
Lack of fit	0.0742	3	0.9632	0.4918	**not significant**	0.0116	3	1.70	0.3039	**not significant**
Pure error	0.1027	4				0.0091	4			
Cor Total	14.97	16				2.79	16			

Result analysis

Breakage rate analysis

The variance analysis of the breakage rate shows that the P-value of the model significance test is less than 0.05, indicating that the obtained regression mathematical model has a high degree of correlation with the experimental results. The regression equation of the breakage rate in relation to the experimental factors was derived through multiple regression analysis as follows:

$$Y_1 = 2.57 + 1.07A + 0.47B + 0.1587C + 0.2075AB + 0.285AC + 0.2725BC + 0.681A^2 + 0.1335B^2 + 0.406C^2 \quad (20)$$

The response surfaces of each test factor affecting the breakage rate are shown in Fig. 20. Among the primary factors, drum speed (A) and deflection angle (B) exert a highly significant influence on the maize threshing breakage rate, while feeding rate (C) has a significant effect. From the contour line density and the shape of the response surfaces, it can be observed that when either the deflection angle (B) or the feeding rate (C) is held constant, variations in drum speed (A) produce densely distributed contour lines and the steepest interaction surfaces. This indicates that drum speed (A) has the greatest effect on the breakage rate, followed by the deflection angle (B), while the feeding rate (C) has the least influence. Regarding factor interactions, the AC interaction has a highly significant effect on the breakage rate of the threshing device, whereas the AB and BC interactions exhibit significant effects, consistent with the variance analysis results for breakage rate.

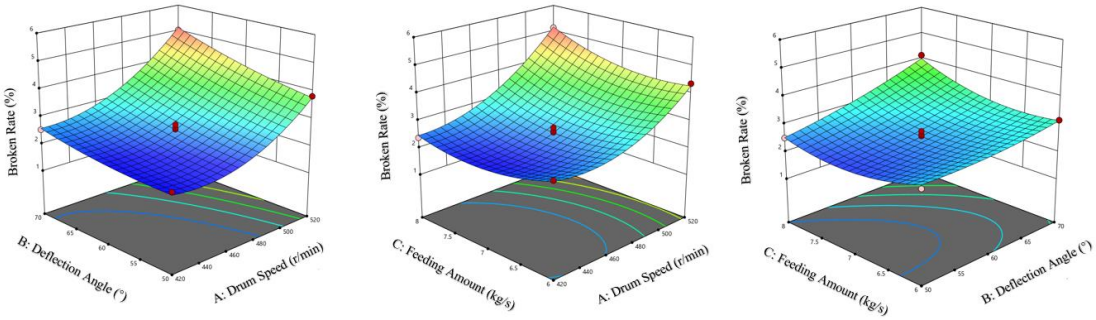

Fig. 20 - Response surface of the breakage rate

Analysis of unthreshed rate

According to the variance analysis of the unthreshed rate, the P-value of the model significance test is less than 0.05, indicating that the regression mathematical model obtained exhibits a high degree of fit with the experimental results.

The regression equation describing the relationship between the unthreshed rate and the experimental factors was derived through multiple regression analysis as follows:

$$Y_1 = 0.238 - 0.4312A - 0.305B + 0.0838C + 0.2725AB - 0.065AC - 0.0875BC + 0.096A^2 + 0.1035B^2 + 0.091C^2 \quad (21)$$

The response surface illustrating the effects of each test factor on the unthreshed rate is shown in Fig. 21. Among the primary factors, drum speed (A), deflection angle (B), and feeding rate (C) all exert highly significant influences on the maize threshing performance. Based on the contour line density and the shape of the response surface, it can be observed that when the feeding rate (C) is held constant, the contour lines become denser as the drum speed (A) and deflection angle (B) vary. This indicates that drum speed (A) and deflection angle (B) have the greatest impact on the unthreshed rate, while feeding rate (C) exerts the least effect. Regarding the interaction terms, the AB interaction shows a highly significant influence on the unthreshed rate of the threshing device, whereas the AC and BC interactions exhibit significant effects - consistent with the results of the variance analysis for unthreshed rate.

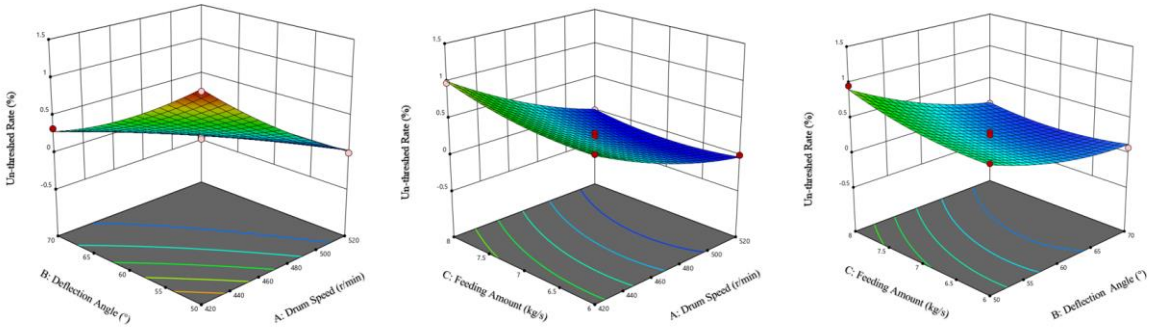

Fig. 21 - Response surface of unthreshed rate

Parameter optimization and verification test

Using Design-Expert software, the experimental results were analysed to optimize the parameters of the designed double-drum maize threshing device, targeting the maximum threshing rate and minimum breakage rate, with priority given to minimizing the unthreshed rate. After rounding, the optimized parameters were determined as follows: drum speed of 453 r/min, deflection angle of 69°, and feeding rate of 6.7 kg/s. Under these conditions, the predicted breakage rate and unthreshed rate were 2.706% and 0.118%, respectively.

According to the optimization results, verification tests were conducted, and the average of three replicates was taken as the final result. The measured breakage rate was 2.76%, and the unthreshed rate was 0.11%. The small deviation between the experimental and predicted values confirms the high reliability and accuracy of the optimization model.

DISCUSSION

In this study, a tangential-transverse axial-flow double-drum threshing device equipped with a flexible concave sieve was developed. A buffer spring was incorporated into the fixed concave sieve, designed based on the average kernel crushing force of 252 N, to effectively absorb impact forces from maize ears and enable adaptive adjustment of the threshing gap during high or uneven feed rates. Under conditions of high moisture content (30% ± 1%) and dense planting, the kernel damage rate was 2.76%, which is below the national standard limit (≤ 5%) (SAC/TC 201, 2017) and significantly lower than the average damage rate of 8.34% typically observed during grain harvesting in Southwest China (*Zhao et al., 2020*). The unthreshed rate was 0.11%, representing a 78.8% reduction compared with the flexible threshing device developed by Chen et al. (2020) for high-moisture maize kernels (unthreshed rate = 0.52%). These results demonstrate the superior performance of the proposed design and provide a valuable reference for the development of maize threshing devices adapted to the conditions of Southwest China.

In the tangential-transverse axial-flow double-drum threshing device developed in this study, the diameters of the tangential and transverse drums are identical. Future research can focus on multi-objective optimization involving different drum diameters and speed ratios. Since the tangential drum primarily performs pre-threshing and breaks up kernel clusters, its performance has a significant influence on the threshing efficiency of the subsequent transverse axial-flow drum. Enhancing the pre-threshing capability of the tangential drum could further improve overall threshing efficiency and reduce the machine's overall size.

The EDEM-ADAMS coupling simulation verified that the flexible concave sieve effectively reduces grain damage during operation. The vertical spacing between the drums and the configuration of the transition plate were determined through simulation, providing a theoretical basis for prototype construction. The middle section of the maize ear used in this study exhibits a uniform kernel arrangement and full grain development, making it representative of the entire ear (*Yu et al., 2021*). However, minor structural differences exist between the ear's tip and base. Therefore, future work should aim to establish a more comprehensive discrete element model of the entire maize ear to support the further development and optimization of maize threshing devices.

CONCLUSIONS

The main findings of the study are as follows:

(1) Based on the structural characteristics of maize and its kernel arrangement pattern, the key factors influencing the threshing and breakage behaviour of high-moisture-content maize were identified through theoretical analysis. The combination mode of the double-drum threshing device was determined, and through theoretical and EDEM simulation analysis, the optimal vertical height difference between the tangential and transverse drums was found to be 25 mm. A vertical transition plate was established to ensure smooth material transport between the drums.

(2) By analysing the forces and motion interactions between the concave sieve, threshing elements, and maize ears, the stiffness of the buffer spring was calculated to be 9 N/mm. A discrete element model of the middle section of the maize ear was constructed, and a coupled MBD–DEM simulation was performed.

(3) A response surface methodology (RSM) test was conducted using drum speed, deflection angle, and feeding rate as test factors, with breakage rate and unthreshed rate as evaluation indices. Regression models were developed for both response variables. By prioritizing minimization of the unthreshed rate, the optimal parameter combination was determined as: drum speed = 453 r/min, deflection angle = 69°, and feeding rate = 6.7 kg/s. Validation tests showed a breakage rate of 2.76% and an unthreshed rate of 0.11%, closely matching the predicted model values, confirming the reliability of the optimization results.

ACKNOWLEDGEMENT

This research was funded by the Science and Technology Department of Sichuan Province (No. 2020YFQ0033) through the project "Research and Demonstration of Machinery and Equipment for Critical Processes in Maize -Soybean Strip Intercropping Systems".

REFERENCES

[1] Cui, T., Fan, C., Zhang, D., Yang, L., Li, Y., Zhao, H., (2019). Research Progress of Maize Mechanized Harvesting Technology (玉米机械化收获技术研究进展分析). *Transactions of the Chinese Society of Agricultural Machinery*, 50(12). https://doi.org/10.6041/j.issn.1000-1298.2019.12.001.

[2] Han, D., Zhou, Y., Nie, J., Li, Q., Chen, L., Chen, Q., Zhang, L., (2024). DEM model acquisition of the corn ear with bonded particle model and its simulated parameters calibration, *Granular Matter*, 26(2), p.54. https://doi.org/10.1007/s10035-024-01427-1.

[3] Li, H., Wang, Q., Ma, J., Wang, Y., Yue, D., Geng, D., (2023). Design and experiment of transverse axial flow corn flexible threshing device, *INMATEH Agricultural Engineering*, pp. 461–470. https://doi.org/10.35633/inmateh-69-43.

[4] Yang, L., Wang, W., Zhang, H., Li, L., Wang, M., Hou, M., (2018). Improved Design and Bench Test Based on Tangential Flow-Transverse Axial Flow Maize Threshing System (切流-横轴流玉米脱粒系统改进设计及台架试验). *Transactions of the Chinese Society of Agricultural Engineering*, 34(1), pp. 35–43. https://doi.org/10.11975/j.issn.1002-6819.2018.01.006.

[5] Chen, M., Xu, G., Wang, C., Diao, P., Zhang, Y., Niu, G., (2020) Design and Experiment of Roller-type Combined Longitudinal Axial Flow Flexible Threshing and Separating Device for Corn (纵轴流辊式组合玉米柔性脱粒分离装置设计与试验). *Transactions of the Chinese Society for Agricultural Machinery*, 51(10), pp. 123–131. https://doi.org/10. 6041 / j. issn. 1000-1298. 2020. 10. 014.

[6] Poustovit S. V. and Katkov V. I. (2016) Research of Process Threshing Kolosov Woroch. *Bulletin of Uman National University of Horticulture.*, (2), pp. 38–41.

[7] SAC/TC 201 (2017) 'Thresher—Testing method'. Available at: https://kns.cnki.net/KCMS/detail/detail.aspx?dbcode=SCSF&dbname=SCSF&filename=SCSF00053299 (Accessed: 7 March 2025).

[8] SAC/TC 201 (2020) 'Corn Combine Harvester'. Available at: https://kns.cnki.net/KCMS/detail/detail.aspx?dbcode=SCSF&dbname=SCSF&filename=SCSF00065680 (Accessed: 7 March 2025).

[9] Steponavičius, D. Dainius, S., Aurelija, K., Valdas, K., Karolis, Z., (2017) Analysis of Corn Ears Movement within the Threshing Crescent Using High-Speed Recording Method. *Journal of Measurements in Engineering*, 5(4), pp. 240–248. https://doi.org/10.21595/jme.2017.19457.

[10] Steponavičius, D., Pužauskas, E., Špokas, L., Jotautienė, E., Kemzūraitė, A., Petkevičius, S., (2018) Concave Design for High-Moisture Corn Ear Threshing. *MECHANIKA*, 24(1), pp. 80–91. https://doi.org/10.5755/j01.mech.24.1.18345.

[11] Wang, K., Xie, R., Ming, B., Hou, P., Xue, J., Li, S., (2021) Review of combine harvester losses for maize and influencing factors. *International Journal of Agricultural and Biological Engineering*, 14(1), pp. 1–10. https://doi.org/10.25165/j.ijabe.20211401.6034.

[12] Wang, P., Jin, C., Wang, C., Li, P., Zhao, Z., (2023) Research status of threshing system of grain combine harvester (谷物联合收获机脱粒系统研究现状). *Journal of Chinese Agricultural Mechanization*, 44(5), pp. 48–57. https://doi.org/10.13733/j.jcam.issn.2095-5553.2023.05.007.

[13] Wang, R., Zhao, X., Ji, J., Jin, X., Li, B., (2021) Design and performance analysis of tangential-axial flow threshing device for oat harvester. *International Journal of Agricultural and Biological Engineering*, 14(6), pp. 61–67. https://doi.org/10.25165/j.ijabe.20211406.6173.

[14] Xing, S., Cui, T., Zhang, D., Yang, L., He, x., Li, C., Dong, J., Jiang, Y., Wu, W., Zhang, C., Du, Z., (2024) Design and optimization for a longitudinal-flow corn ear threshing device of low loss and low energy consumption. *Computers and Electronics in Agriculture*, 226, p. 109328. https://doi.org/10.1016/j.compag.2024.109328.

[15] Li, X., Liu, Y., Du, Z., Ma, Y., Gen, L., Ma, F., (2014) Experimental Effect of Arrangement Law of Corn Ear Kernels on the Discrete Performance (玉米果穗籽粒组砌规律对其离散效果的影响). *Journal of Agricultural Mechanization Research*, 36(10), pp. 186–191. https://doi.org/10.13427/j.cnki.njyi.2014.10.045.

[16] Li, X., Liu, Y., Ma, Y., Du, Z., Ma, F., (2015) Effect of Gap Direction Among Corn Ear Kernels on the Circulating Dint Decline (玉米果穗籽粒间缝隙走向对其循环力衰败的影响). *Journal of Agricultural Mechanization Research*, 37(1), pp. 183–187. https://doi.org/10.13427/j.cnki.njyi.2015.01.043.

[17] Li, X., Zhang, W., Xu, S., Du, Z., Ma, Y., Ma, F., Liu, J., (2023) Low-Damage Corn Threshing Technology and Corn Threshing Devices: A Review of Recent Developments. *Agriculture*, 13(5), p. 1006. https://doi.org/10.3390/agriculture13051006.

[18] Li, X. & Ma, L. (2017) Analysis of Finite Element Method on Dynamic Contact of Corn Ear (玉米果穗动力接触的有限元分析). *Journal of System Simulation*, 29(1), pp. 67–75. https://doi.org/10.16182/j.issn1004731x.joss.201701010.

[19] Zhou, X., Li, X., Gao, L., Liu, M., (2005) Comparison of Corn Kernel Damage Using Two Types of Threshing Cylinders (两种脱粒滚筒的玉米籽粒损伤试验研究). *Journal of Shenyang Agricultural University*, 36(6), pp. 756–758. https://doi.org/10.3969/j.issn.1000-1700.2005.06.030.

[20] Yu, Y., Li, L., Zhao, J., Wang, X., Fu, J., (2021) Optimal Design and Simulation Analysis of Spike Tooth Threshing Component Based on DEM. *Processes*, 9(7), p. 1163. https://doi.org/10.3390/pr9071163.

[21] Yu, Y., Fu, H., & Yu, J., (2015) DEM-Based Simulation of the Corn Threshing Process. *Advanced Powder Technology*, 26(5), pp. 1400–1409. https://doi.org/10.1016/j.apt.2015.07.015.

[22] Zhao, B., Li, X., Zhou, M., Song, B., Lei, E., Li, Z., Wu, Y., Yuan, J., Kong, F., (2020) Current status and influencing factors of broken rate in mechanical grain harvesting of maize in Southwest China (西南玉米机械粒收籽粒破碎率现状及影响因素分析). *ACTA AGRONOMICA SINICA*, 46(1), pp. 74–83. https://doi.org/10.3724/SP.J.1006.2020.93026.

[23] Wang, D., Cui, T., Zhang, D., Yang, L., He, X., Zhang, Z., (2021) Design and Experiment of Rasp Bar Threshing Element of Corn Combine Harvester (玉米联合收获机纹杆式脱粒元件设计与试验). *Transactions of the Chinese Society for Agricultural Machinery*, 52(9), pp. 115–123. https://doi.org/10.6041/j.issn.1000-1298.2021.09.013.